

PREPARATION AND CHARACTERIZATION OF VERNOLIC ACID METHYL ESTER FUNCTIONALIZED ORDERED MESOPOROUS MATERIALS

Yonas Chebude^{1*}, Gutta Gonfa² and Isabel Díaz³

¹Chemistry Department, Addis Ababa University, P.O. Box 1176, Addis Ababa, Ethiopia

²Chemistry Department, College of Natural Sciences, P.O. Box 378, Jimma, Ethiopia

³Instituto de Catálisis y Petroleoquímica, CSIC, C/Marie Curie 2, 28049 Madrid, Spain

(Received October 5, 2022; Revised December 26, 2022; Accepted December 31, 2022)

ABSTRACT. Vernonia oil is a naturally epoxidized triglyceride oil extracted from the seed of *Vernonia galamensis*, a native plant in East Africa. After hydrolysis to vernolic acid (VA) and derivatization, vernolic acid methyl ester (VAME) is synthesized and used to functionalize ordered mesoporous materials (OMM). Al-MCM-41 with Si/Al ratio of 15, pure silica SBA-15 and periodic mesoporous organosilica (PMO) are employed as supports exploring the different surface properties. Following optimization of the VAME/OMM ratios, selected samples, i.e. those with 13% VAME, were impregnated with AgNO₃ in NaBH₄ to obtain Ag-nanoparticles. The final AgVAME-OMM potential catalysts were characterized by transmission electron microscopy, observing an efficient loading of Ag nanoparticles in pure silica SBA-15 with VAME with 500 m² specific surface area and 6 nm pore size.

KEY WORDS: Vernolic acid methyl ester, Vernonia oil, Functionalization, Ordered mesoporous materials, Catalysis

INTRODUCTION

Since the first ordered mesoporous materials (OMMs) were discovered nearly thirty years ago, many novel approaches have been successfully implemented in designing the synthesis and modification of a large number of silica and non-silica materials with the aim of tuning their constitutional and morphological properties. OMMs have found practical applications in catalysis, gas separation and adsorption techniques, medicine, in the electronics industry and other related fields [1]. Therefore, changing their constitutional and morphological properties will result in increasing their activities and selectivity through the functionalization of their large surface areas (> 1000 m²g⁻¹) and internal frameworks [2].

Functionalization of OMMs is usually performed via grafting or post-modification methods with inorganic/organic components, i.e. acids, bases, metallic nanoparticles, organometallic complexes and composite materials [3]. The functionalization of mesoporous materials increases their hydrophobicity and hydrothermal stability. In this regard, several attempts have been undertaken on the surface modification of mesoporous silica using long alkyl chains of fatty acids such as oleic acid and its derivatives [4]. Functionalized mesoporous materials have shown to have potential applications as hard templates to control the shape and size of metal nanoparticles that can be used as catalysts [5] and in biomedicine for drug delivery systems [6].

As reported in the literature, a facile synthesis of oleic acid and imidazole containing ligands conjugated to fatty acids chains between oleic acid and 2-mercaptoimidazole and condensation between (4)5-imidazoledithiocarboxylic and 9,10-epoxystearic acids were used as surface ligands for stabilization of nanocrystals and metal nanoparticles for catalytic applications [3, 7-9]. Vernonia oil is a bio-renewable feedstock extracted from the seeds of *Vernonia galamensis*, a plant native to East Africa [10]. The extract contains a significant concentration (approx. 40%) of naturally epoxidised triglyceride oils. This natural functionality would allow for more facile exploitation of vernolic acid in possible future applications as opposed to other commonly-used fatty acids such as oleic acid, which generally must be epoxidised before undergoing further

*Corresponding author. E-mail: yonas.chebude@aau.edu.et

This work is licensed under the Creative Commons Attribution 4.0 International License

reactions [11]. Oils of this type are particularly useful as cross-linking agents in environmentally benign, solvent-free powder coatings and bonded structural materials. Of more interest, in a sense of chemistry research, is the application of these materials as building blocks for the preparation of biodegradable hydrophobic plastics including polyhydroxy alkanooates (PHAs), which exhibit high performance barrier properties. Moreover, derivatives of vernonia oil offer great potentials in pharmaceuticals (topical medical preparations) [12, 13].

In the course of our work, a vernolate starch ester has been synthesized via the enzymatic esterification of cassava starch in a mixture of organic solvent and ionic liquid (IL) as reaction medium as well as Novozyme 435 as the catalyst. The IL based medium imparts high solubility and significant activity of the enzyme [14]. In the optimized reaction conditions, a degree of substitution (DS) of 0.95 was achieved, at a reaction temperature of 40 °C within 72 h, which indicates that the enzymatic reaction might be specific towards the hydroxyl groups of the starch backbone. The development of drug delivery systems (DDS) using hyperbranched biopolymers (HBP) has recently made huge progress and in this regard, vernonia oil based HBPs have several advantages over other epoxidized vegetable oils produced industrially and it is believed that vernonia oil will continue to be a very attractive raw material for many applications [15].

In this work, we report the use of vernolic acid methyl ester (VAME) for surface modification of three types of ordered mesoporous materials, i.e. Al-MCM-41, SBA-15 and periodic mesoporous organosilica (PMO), which are subsequently used for immobilization of silver nanoparticles (Ag-NPs) due to its potential for catalytic applications, for instance in the photocatalytic degradation of dyes produced in the textile industry.

EXPERIMENTAL

Extraction and purification of vernonia oil: Hydrolysis to vernolic acid and derivatization to vernolic acid methyl ester (VAME)

Vernonia galamensis seeds have high oil content of 40-42%, which can be obtained via the conventional solvent extraction method as described hereunder. *V. galamensis* seeds were first sun-dried, cleaned and cooled in a refrigerator, heated in an oven for about 1 hour at 363 K for lipase deactivation, and ground in a coffee mill grinder. Powdered seeds of *V. galamensis* were extracted with n-hexane as a solvent for three hours using a Soxhlet extraction system. The crude vernonia oil (CVO) was filtered, kept overnight in a refrigerator and decanted to separate the oil from the solid residue and then the solvent was removed using a rotary evaporator. After the extraction of crude vernonia oil, non-triacylglycerol components were removed from the crude oil by solid phase extraction (SPE). In this procedure, 10-20 g of CVO was dissolved in 10-20 mL n-hexane and mixed with 35% w/w activated carbon introduced from the top of 60 g packed silica gel. Three different fractions were collected by elution with n-hexane (50-60 mL, fraction 1), 1:1 v/v of n-hexane/diethyl ether (60 mL, fraction 2) and methanol (40 mL, fraction 3), respectively to get glycerides and non-glycerides separated. This was followed by deacidification by solvent extraction with n-hexane/ diethyl ether. The purity of the purified vernonia oil (VO) was checked by TLC, ¹H and ¹³C-NMR as well as FT-IR analyses.

For the hydrolysis of VO, 50 mL methanol and 0.125 mol (5 g) sodium hydroxide were placed in a 250 mL round-bottom flask with a magnetic stirrer bar. The flask was fitted with a condenser and the mixture was heated to reflux while stirring for about 30 min until complete dissolution of the sodium hydroxide. 5.53 mmol (5.12 g) vernonia oil was added to the flask. The resulting brownish solution was refluxed with continuous stirring for about 30 min. The solution was then immediately transferred to a beaker and allowed to form a semi-solid product on cooling. About 100 g of ice and 50 mL of water were added. The cold mixture was filtered under a reduced pressure to obtain a white solid soap. The soap was transferred into a beaker and mixed with 100

g ice and 100 mL water, acidified with 4 mL glacial acetic acid. The acidified mixture was immediately filtered under reduced pressure, followed by hexane extraction (100 mL). After the removal of the aqueous phase and drying over magnesium sulfate, the excess solvent was removed under reduced pressure. Purification of the vernolic acid was accomplished by recrystallisation from hexane at 195 K. After filtration under reduced pressure, the vernolic acid was rinsed with cold hexane. The pure vernolic acid, a yellow solid that melts with a yield of about 60% at room temperature was obtained.

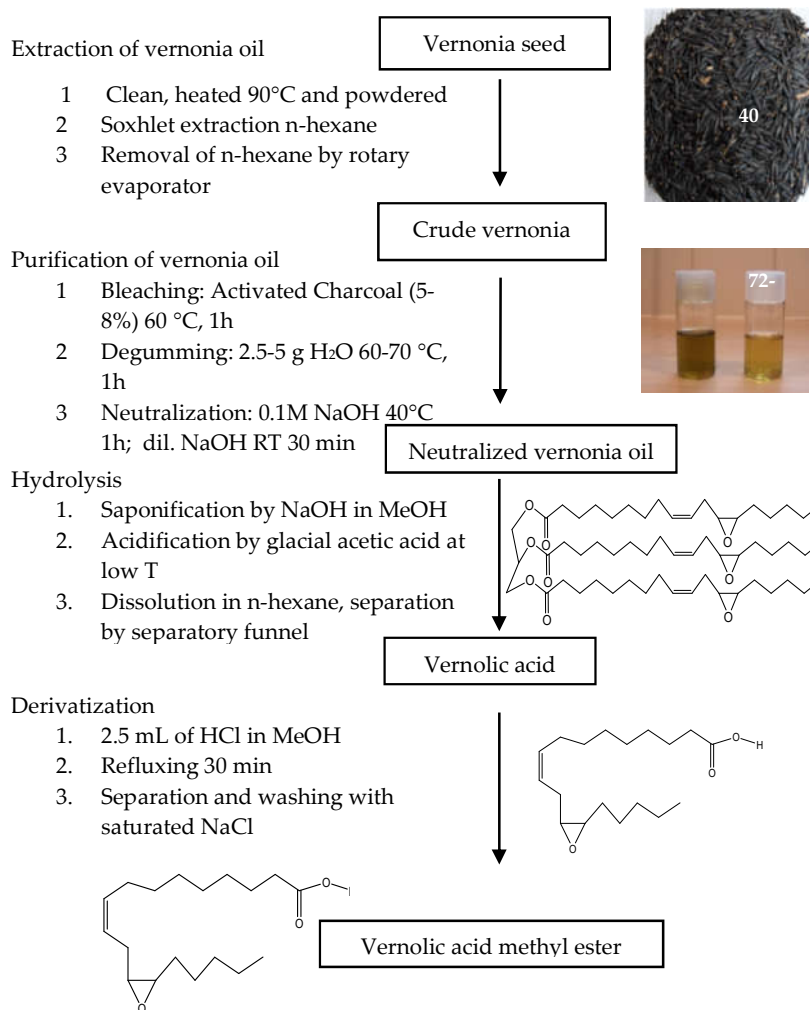


Figure 1. Process flow for the extraction and purification of vernonia oil: Hydrolysis to vernolic acid (VA), and derivatization to vernolic acid methyl ester (VAME).

Preparation of vernolic acid methyl ester (VAME) was performed by esterification of vernolic acid [16, 17]. First, methanolic hydrochloride acid solution was prepared by adding 2.5 mL of

acetyl chloride to 50 mL of methanol in an ice bath and the mixture was left closed for 15 min. Vernolic acid was esterified in the absence of diethyl ether. After cooling, the refluxed solution was transferred into a separatory funnel and mixed with 10-15 mL saturated NaCl solution. It was then washed twice with 10 mL diethyl ether, and the lower phase was discarded. Finally, the diethyl ether phase was washed with 5-10 mL saturated NaCl solution and dried with 0.5 g sodium sulfate for 30 min, which was then separated from the solvent under vacuum drying. The entire process is summarized in Figure 1.

Surface modification of OMMs with VAME

Different proportions of VAME and OMM were tested in order to optimize the final composite. In a typical procedure, n-hexane and VAME were mixed with stirring, and then an appropriate amount of OMM was added. The mixture was heated under stirring at 60 °C for 4 h. The solution was filtered and the precipitate was rinsed thoroughly with ethanol and deionized water. The precipitate was kept in a vacuum desiccator for 24 h. The samples were labeled as VAME-OMM-n, where “n” corresponds to increasing VAME/VAME+OMM(g).

Loading of Ag on VAME-OMMs

After optimization of the VAME/OMM ratios, selected samples, i.e. only those with 13% VAME, were impregnated with Ag nanoparticles. The procedure was adapted from the literature [18, 19]. Hence, 0.15 g of VAME-OMMs were suspended in 15 mL of DMF solution of 1.2 g AgNO₃. The mixture was equilibrated by stirring for 12 h. Freshly prepared DMF solution of 120 mg of NaBH₄ in 15 mL DMF was added to the mixture dropwise at a reduced temperature (3–5 °C) with constant stirring. The addition of NaBH₄ is followed by UV Vis spectroscopy to follow the formation of silver nanoparticles. The mixture was then further stirred for 2 h. Then it was filtered, washed with acetone, vacuum dried and labeled as AgVAME-OMM.

Characterization of the materials

X-ray diffraction (XRD) patterns were collected with a X'Pert Pro PANalytical diffractometer (CuK α radiation, $\lambda = 0.15406$ nm). Thermogravimetric analysis (TGA) was performed using a Perkin-Elmer TGA7 instrument, with a heating rate of 20 °C/min under air flow. Nitrogen adsorption-desorption isotherms were measured in a Micromeritics ASAP 2420 physisorption analyzer and the samples were degassed at 350 °C and 150 °C in the case of the loaded samples, for 16 h prior to data collection. Specific surface area was estimated by BET method, external/micropore surface area by t-plot method, and pore size distribution (PSD) by BJH method. Transmission Electronic Microscopy (TEM) images were registered with a JEOL 2100F instrument operating at 200 kV. The samples were gently crushed, and mounted directly on a holey carbon Cu-grid.

RESULTS AND DISCUSSION

Results on vernonia oil hydrolysis to vernolic acid and derivatization to vernolic acid methyl ester (VAME).

Vernonia oil was first obtained by extraction of crude vernonia oil (40% yield) and then the crude vernonia oil was purified into deep golden yellow neutral vernonia oil via conventional methods (bleaching, degumming and neutralization) as described in the Experimental section and summarized in Figure 1. The final purified vernonia oil was fully characterized by ¹H and ¹³C NMR as well as FT-IR spectroscopy resulting in the identification of the major functional groups:

the ester, the double bond and the epoxy of the triglyceride structure [15]. Further hydrolysis allows obtaining the vernolic Acid which was also easily identified by ^1H and ^{13}C NMR. Figure 2 shows the spectra and Table 1 collects the main peaks with the corresponding identifications. The presence of hydroxyl proton (-OH) confirmed the success of the hydrolysis of vernonia oil.

Vernolic acid methyl ester (VAME) was synthesized according to procedure reported in the literature [16, 17] via acid catalyzed esterification reaction starting from the VA. The resulted compounds were purified by column chromatographic separation based on TLC purity test obtaining a recovery yield of VAME of 45%. NMR studies, ^1H and ^{13}C NMR were used to follow the esterification process, the plots are included in Figure 2 and the main peak assignments are collected in Table 1. ^1H NMR spectrum of VAME could identify the presence of major functional groups. The integral peak areas of double bond, epoxy and methyl functional groups of VAME are 1, 0.83 and 1.67, respectively compared to 1, 1, and 1.5 of their theoretical values for VAME. The epoxy group has undergone partial ring opening, due to partial epoxy ring opening by HCl catalyst that in turn introduces chloro and hydroxo substituent, respectively. This is also the main reason of intensity reduction in the epoxy protons signal. Similarly, the ^{13}C NMR spectrum shows the main functional groups of the methyl ester as the data indexed in Table 1. Apart from the given data the new peaks appear at 67.41-67.88 and 73.44 ppm, respectively. This may be due to the hydroxo and chloro substituents resulted from partial ring opening of epoxy group whose intensity is diminished.

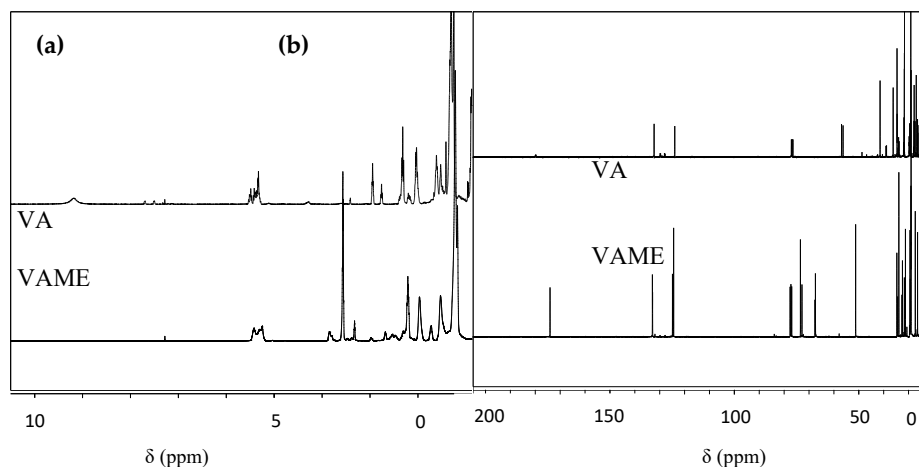


Figure 2: (a) ^1H NMR spectra of vernolic acid (VA) and vernolic acid methyl ester (VAME) (δ ppm, 400 MHz, CDCl_3). (b) ^{13}C NMR spectra of vernolic acid (VA) and vernolic acid methyl ester (VAME) (δ ppm, 400 MHz, CDCl_3).

Results on surface modification of Al-MCM-41, SBA-15 and PMO with vernolic acid methyl ester (VAME).

Surface modification was done with vernolic acid methyl ester (VAME) so as to introduce surface ligands with increased hydrophobicity to further immobilize silver metal nanoparticles [20].

In a first set of experiments, several ratios were tested in order to optimize the relationship between the amount of VAME and the porosity in the final composite. The best ratio for VAME loading would be the one that allows surface modification of the OMM while avoiding pore blocking or complete loss of pore volume. At the same time, the nature of the pore wall of the

OMM will determine an optimum surface chemistry for efficient loading of silver. Acid OMM, Al-MCM-41 with Si/Al ratio of 15 with mild Lewis acidity offers anchoring sites for Ag [21]. Pure silica SBA-15 was chosen due to the larger pore size (> 8 nm) and the presence of silanol groups on the surface for potential anchoring [22]. Finally, a periodic organosilica formed with ethylene groups in the pore wall was chosen as an hydrophobic support in which the adsorption of the vernolic acid methyl ester may be favored by simple hydrophobic interactions [23].

Table 1. Data of ^1H and ^{13}C NMR spectra of vernolic acid (VA) and vernolic acid methyl ester (VAME).

Type of proton ^1H NMR	δ (ppm)	Type of Carbon ^{13}C NMR	δ (ppm)
Vernolic acid (VA)			
Hydroxylic (-OH)	9.17-9.20	Carbonyl (O=C)	179.83-179.96
Olefinic (-CH=CH-)	5.33-5.49	Olefinic (CH=CH)	123.93-132.26
Epoxy (-O-C-H)	2.74-2.95	Epoxy (O-C-H)	56.31-56.92
Methylene olefinic (-CH ₂ -CH=CH-CH ₂ -)	2.02-2.32	Methylene chain (CH ₂) _n	22.67-34.62
Methylene chain (CH ₂) _n	1.25-1.61	Methyl (CH ₃)	13.81
Methyl (CH ₃)	0.87		
vernolic acid methyl ester (vame)			
Olefinic (-CH=CH-)	5.20-5.40	Vernonyl Carbonyl (O=C)	174.05
Methoxy (-OCH ₃)	3.65-3.66	Olefinic (CH=CH)	124.39-132.92
Epoxy (-O-C-H)	2.61-2.76	Epoxy (O-C-H)	57.86
Methylene (-CH ₂ -CH=CH-CH ₂ -)	2.04-2.31	Methoxy (-OCH ₃)	51.26
Methylene (-CH ₂) _n	1.25-1.30	Methylene (CH ₂) _n	22.4-33.39
Methyl (CH ₃)	0.89	Methyl (CH ₃)	13.88

In an attempt to quantify the loaded VAME in the OMMs and determine its thermal stability, the composites were characterized by thermogravimetric analysis (TGA/DTG). Table 2 collects the different ratios of VAME versus OMMs as well as the different weight losses and Figure 3 plots the TGA/DTG curves of the three series.

Table 2. VAME loaded samples using several ratios in the three supports: Al-MCM-41, SBA-15 and PMO.

VAME-OMM-x	X = VAME/ (VAME+OMM)	TGA weight loss (%)			T > 150 °C weight loss (%)
		T < 150 °C	150-600 °C	T > 600 °C	
VAME-MCM-1	0.13	9.97	12.68*	6.14	18.82
VAME-MCM-2	0.18	11.08	9.44*	4.92	14.36
VAME-MCM-3	0.59	3.00	36.92*	12.25	49.17
VAME-MCM-4	0.78	3.34	36.61*	12.55	49.16
VAME-SBA-1	0.13	5.73	5.90	0.96	6.86
VAME-SBA-2	0.18	5.03	3.86	1.25	5.11
VAME-SBA-3	0.59	1.18	33.04	1.62	34.66
VAME-SBA-4	0.78	1.80	40.63	1.16	41.79
VAME-PMO-1	0.13	9.27	12.02	6.23	11.98**
VAME-PMO-2	0.18	3.07	43.10	6.86	43.69**
VAME-PMO-3	0.59	3.07	46.95	4.09	44.77**
Parent PMO					6.27**

* For the Al-MCM-41 series of samples, this range is 150 to 500 °C, where the derivative (DTG) shows the end of the main weight loss as it can be observed in Figure 2(a). ** 6.27% corresponds to the organic groups forming the walls of PMO. This value has been subtracted from the values of the PMO series.

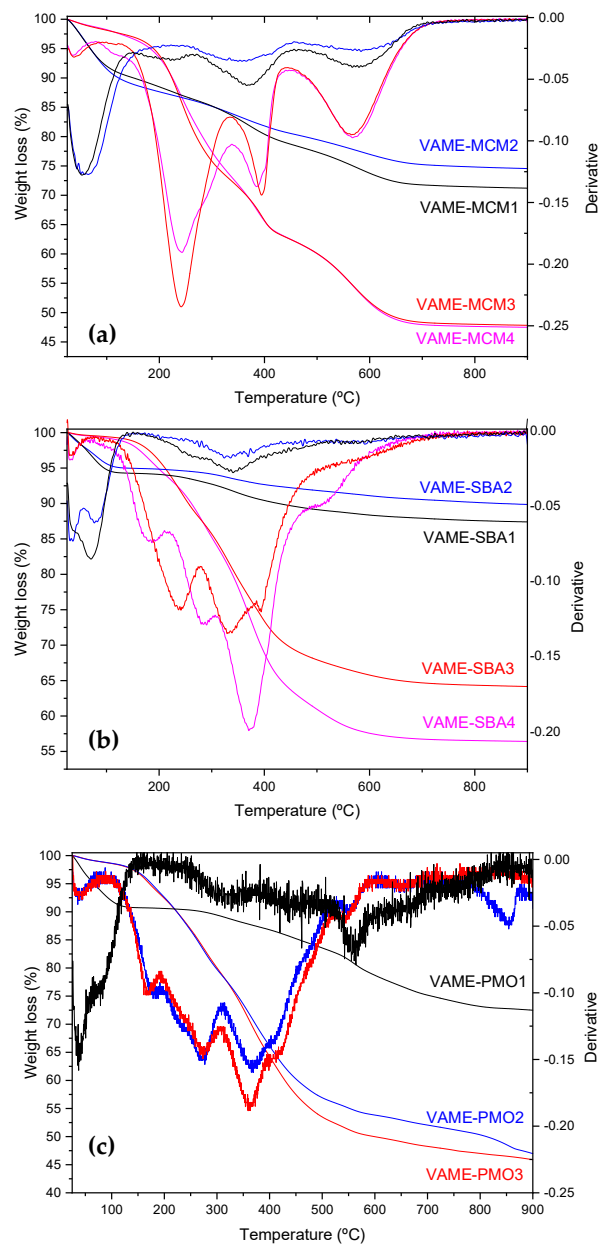


Figure 3. Thermogravimetric studies, TGA/DTG curves: (a) on Al-MCM-41 (Si/Al =15) series labeled VAME-MCM-x; (b) pure silica SBA-15 series labeled as VAME-SBA-x; and (c) organosilica PMO series VAME-PMO-x.

In all the TGA curves, the weight loss observed below 150 °C corresponds to solvent or water desorption remaining from the loading procedure. A mid range prominent weight loss is observed in the three series up to 500 °C in the case of Al-MCM-41 and 600 °C in the SBA-15 and PMO series. The weight loss above 500 or 600 °C can be affected by the desorption of water or organic species derived from the decomposition of the supports. Nevertheless, this last step is included in the estimation of VAME incorporation as the difference is not clear enough. Table 2 depicts a column of the total weight loss above 150 °C employed to estimate the yield of VAME incorporated compared to the initial VAME/(VAME+OMM) ratios.

For Al-MCM-41, the TGA/DTG curves analysis showed at a glance higher amount of weight loss at $T > 150$ °C being efficiency of VAME loading the highest optimum value for 13% VAME loading. The high value is probably due to the high weight loss of solvent in this sample that may be loaded and released at $T > 150$ °C. In these cases, the third loss centered at $T > 500$ °C may not only be due to the release of water due to silanol condensation but also indicative of some stronger interactions of the VAME with the acid sites of the Al-MCM-41 since this third weight loss shows increasing amount of organic substances as the ratio increases. The most possible interactions between VAME and Al-MCM-41 may be the stronger polar interaction between carboxylic and epoxy functional groups of VAME with acid sites of Al-MCM-41 that lead to much higher loading [24].

In the case of SBA-15 and PMO, higher amount of VAME is expected to be loaded, due to the larger pore sizes of SBA-15 and PMO. The derivatives in these cases are different than in the Al-MCM-41 case, showing that a maximum weight loss (i.e. loading) is achieved around 400 °C, with no weight loss centered at 600 °C. For VAME-SBA, the analysis of TGA/DTG curves shows that there is an increasing total weight loss from approximately 6 to 40 wt % at $T > 150$ °C indicating a higher loading as the VAME/OMM ratio increases. Similarly, for VAME-PMO, the loading is higher as the ratio increases with larger number in this case, ranging from 12 to almost 60 wt% probably due to the higher affinity given the hydrophobicity of PMO. In this case, there is a small weight loss at $T > 600$ °C due to the decomposition of the bridging organic groups of the PMO, which is approximated 6.27 wt% and that has been subtracted from all the modified samples.

In summary, the method seems to be efficient in incorporating VAME regardless of the surface chemistry and pore size of the OMM employed. Thus further studies are required using N_2 adsorption/desorption isotherms to evaluate the optimum ratio for further silver nanoparticles synthesis and catalytic application. The obtained isotherms are plotted in Figure 4 and the textural properties are collected in Table 3.

Table 3. Textural properties obtained from N_2 adsorption/desorption isotherms.

VAME-OMM-x	$X = \text{VAME}/(\text{VAME}+\text{OMM})$	S_{BET} (m^2/g)	Pore volume (cm^3g^{-1})	Pore diameter BJH (nm)
Al-MCM-41		799	1.40	3
VAME-MCM-1	0.13	656.6	1.20	2
VAME-MCM-2	0.18	794.4	1.32	-
VAME-MCM-3	0.59	49.1	0.58	-
VAME-MCM-4	0.78	44.3	0.52	-
SBA-15		609	1.00	8
VAME-SBA-1	0.13	502.2	0.90	6
VAME-SBA-2	0.18	460.1	0.85	6
VAME-SBA-3	0.59	157.2	0.30	-
VAME-SBA-4	0.78	75.2	0.16	-
PMO		882	1.00	7.1
VAME-PMO-1	0.13	588.1	0.68	6
VAME-PMO-2	0.18	15.4	0.08	-
VAME-PMO-3	0.59	15.5	0.09	-

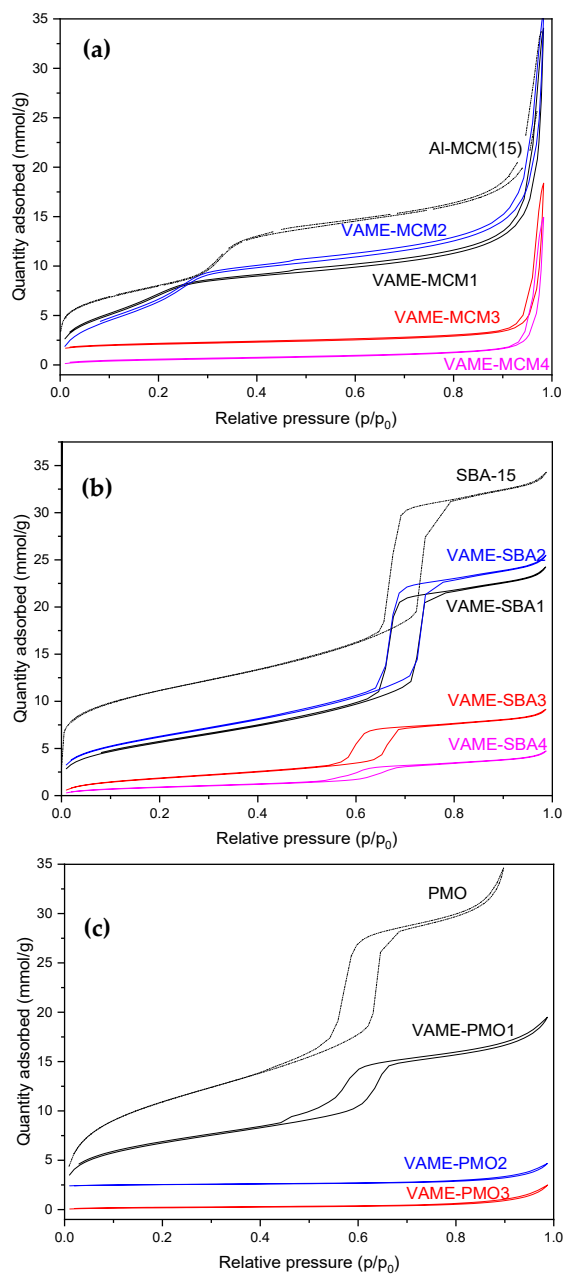


Figure 4. N₂ Adsorption-desorption isotherms of the VAME supported on (a) Al-MCM-41; (b) SBA-15 and (c) PMO.

The isotherms follow type IV as per the IUPAC classification indicating uniform mesopores that are not significantly changed in shape during the modification with VAME, except for the loss of surface area and pore volume. The loading of VAME is obviously diminishing the mesoporosity of the OMMs either by fully filling the channels or simply pore blocking the pore volumes. For Al-MCM-41, as the precursor mass ratio increases from 0.13 to 0.78, the S_{BET} significantly decreased from 799.0 m^2/g in the parent Al-MCM-41 to 656.6 m^2/g in VAME-MCM-1 and to 49 m^2/g in VAME-MCM-3 indicating the total filling of the mesopores. VAME-MCM-2 showed an exception to the trend remaining basically as the original Al-MCM-41. In the case of the SBA-15 series, the relatively larger initial pore size and surface area allows for a larger available surface area even at high VAME/(VAME+OMM) loadings. However, the BJH pore size gives the clue to an optimum support, from 8 nm in the starting SBA-15 to 6 nm in either VAME-SBA-1 or VAME-SBA-2. For PMO series there is a more dramatic decrement in porosity in VAME-PMO-2 and 3, probably due to the higher affinity with VAME leading to pore blockage. VAME-PMO-1 with significantly decreased the BET surface area of almost 300 m^2/g . Yet 6 nm pore size seems to be a good choice for further work.

In summary, the modified materials with optimum 13% VAME loading with highest percent yield of VAME incorporation while maintaining large pore size and surface area seem to be good candidates for encapsulation of Ag nanoparticles with dimension less than the pore size of the modified materials.

Results on Ag loading on VAME/OMMs

Modified OMMs with 13% VAME loading were first impregnated and then reduced as detailed in the Materials and Methods section yielding the final materials labeled: AgVAME-MCM-1, AgVAME-SBA-1 and AgVAME-PMO-1.

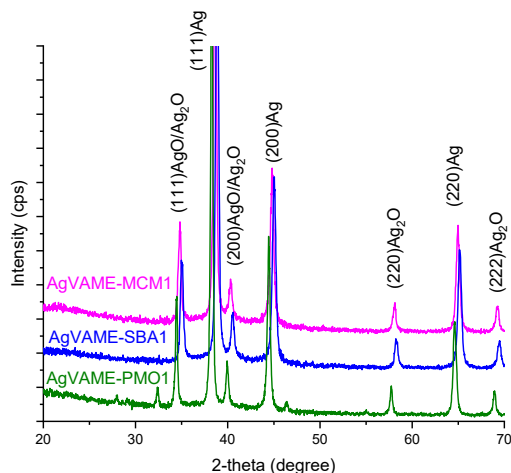


Figure 5. High angle powder XRD of AgVAME-MCM-1 (magenta), AgVAME-SBA15-1 (blue), AgVAME-PMO-1 (green).

The large angle powder X-ray diffraction patterns are plotted in Figure 5. Sharp and intense peaks at 2-theta = 38, 45 and 65 could be indexed as Ag^0 species. Additional low intense peaks at 2-theta = 34, 40, 58 and 69 could be related to the formation of Ag_2O and AgO stabilized species.

These results are consistent with the results reported in literature [18, 19], yet the remaining question is whether the Ag^0 nanoparticles have been efficiently grown inside the porous material, and supported on the VAME. Transmission electron microscopy studies were carried out in order to locate the metal particles and therefore understand if the confined space has played any role in the Ag-impregnation. In the bright field TEM images, the mesopores will be observed due to the contrast pore-wall density, however, the loading of VAME would not be visible due to the very poor scattering power of C-based materials [25].

On the other hand, Ag provides contrast due to its higher electron density, thus, in the images silver particles will show as strong dark contrasts, whereas the mesoporous matrix will show as a pore white- wall-grey contrast scheme. The oxidation state of the silver particles would not be distinguished, therefore, the dark spots may correspond either to Ag^0 or Ag-oxide particles.

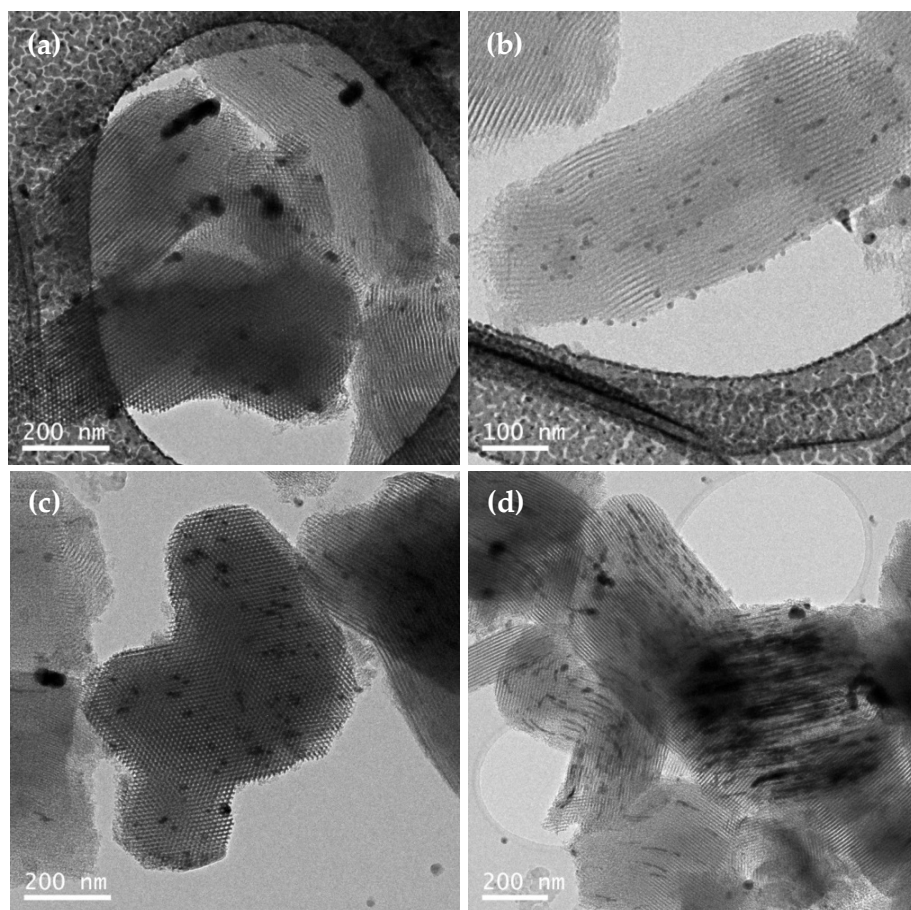


Figure 6. TEM images of the Al-MCM-41 and SBA-15 systems showing: (a) AgVAME-MCM-1 with the orientation parallel to the channels showing the hexagonal arrangement; (b) AgVAME-MCM-1 with the orientation perpendicular to the channels axis. (c) AgVAME-SBA-1 showing hexagonal arrangement; (d) AgVAME-SBA-1 showing the channels with dark filling of Ag species along them.

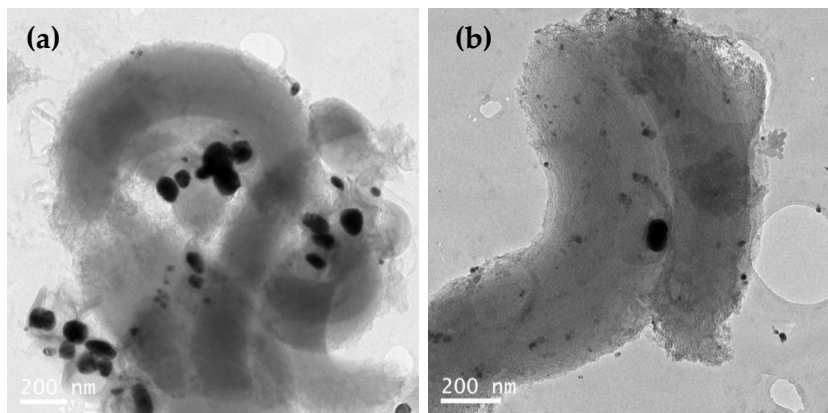


Figure 7. TEM images of the AgVAME-PMO-1 system: (a) low magnification showing large agglomerates of metal particles outside the crystals, and (b) higher magnification showing the channels with almost no pore filling dark contrast.

Figures 6 and 7 show representative images of the three systems. The images retained well-ordered mesoporous channels arranged in a two dimensional hexagonal structure symmetry in all cases. Figure 6(a) and Figure 6(c) allow observing the hexagonal channels arrangement in samples AgVAME-MCM-1 and AgVAME-SBA-1, respectively. In this projection, the electron beam is parallel to the channels showing the pore mouths of the channels, therefore, the dark spot observed filling the mesopores in the honeycomb would correspond to Ag particles filling the channels and projected in the plane of the image. However, this projection may lead to confusion on whether the particles are actually inside filling the pores, or outside and simply on top of the particles leading to the similar contrast effect. In order to clarify this question, the crystals have to be observed in the projection perpendicular to the channels axis to observe the total length of the channels and therefore, the contrast running along them. Figures 6(b) and 6(d) show this projection for samples AgVAME-MCM-1 and AgVAME-SBA-1, respectively. It can be clearly observed in this projection, that in the case of AgVAME-MCM-1 (Figure 6(b)) the majority of the nanoparticles observed are located outside, on the surface of the large particles, although some dark, elongated contrast are also observed in the middle part of the particles, probably indicating that some silver has been efficiently loaded inside the channels. Anyhow, this elongated contrasts due to the formation of Ag particles inside the channels are abundantly and clearly observed in the case of AgVAME-SBA-1 in Figure 6(d). In this case, the surface of the large particles of the mesoporous materials appears clean of silver nanoparticles. Obviously, the larger pore size available in the case of SBA-15, even after surface modification with VAME, offers an optimum surface for the immobilization of the Ag-nanoparticles. The particle size was shown heterogeneous in both systems. Particle size calculated manually using ImageJ software ranges from 2 nm to 40 nm for AgVAME-MCM-1 and the largest size is from 4 nm to 72 nm for AgVAME-SBA-1. Finally, Figure 7 shows representative TEM images for the AgVAME-PMO-1 system where all the silver was clearly aggregated outside the support, forming much larger aggregates leading to conclude that despite the affinity of VAME for PMO support, the combination yields a surface way too hydrophobic for the diffusion of AgNO_3 , leading to a most probably, less efficient immobilization process.

CONCLUSIONS

Derivatives of Vernonia oil are worth investigating as naturally epoxidized triglyceride oil extracted from the seed of *Vernonia galamensis*. In this work, we have worked on the hydrolysis to vernolic acid (VA) and derivatization to vernolic acid methyl ester (VAME) to functionalize ordered mesoporous materials (OMM). The functionalization works efficiently in Al-MCM-41 with Si/Al ratio of 15, pure silica SBA-15 and periodic mesoporous organosilica (PMO) with an optimum of 13% VAME loading that affords certain pore size to further immobilization of active silver nanoparticles. Impregnation with AgNO₃ in NaBH₄ to obtain Ag-nanoparticles was tested in the three modified supports. The final AgVAME-OMM potential catalysts were characterized by transmission electron microscopy, observing that i) Al-MCM-41 is functionalized with VAME efficiently due to the Lewis acidity of the material, yet the Ag nanoparticles are present both inside and outside, probably due to the small pore size; ii) an efficient loading of Ag nanoparticles in pure silica SBA-15 with VAME allows observing only the formation of silver nanoparticles inside the channels given the good textural properties of the modified support (500 m² specific surface area and 6nm pore size); iii) due to the higher affinity between VAME and the hydrophobic walls of PMO, the impregnation in VAME-PMO is not efficient at all, leading to the formation of large Ag agglomerates outside, forming a physical mixture with the support. These observations are corroborated in the preliminary photocatalytic test in the degradation of methyl orange in simulated wastewater showing AgVAME-SBA-1 almost 100% discoloration within 8h, whereas AgVAME-PMO-1 barely showed catalytic activity due to the lack of incorporation of Ag nanoparticles.

ACKNOWLEDGMENTS

This work was funded by the Spanish Agency for International Development Cooperation AECID INNOVACION (2020/ACDE/000373). The authors would like to acknowledge Paul McClory from Vernique Biotech, UK (company dissolved) for the donation of the vernonia seeds.

REFERENCES

1. Szczęśniak, H.; Choma, J.; Jaroniec, M. Major advances in the development of ordered mesoporous materials. *Chem. Commun.* **2020**, 56, 7836-7848.
2. Tüysüz, H.; Schüth, F. Chapter 2: *Ordered mesoporous materials as catalysts* in *Advances in Catalysis*, Vol. 55, Gates, B.C.; Jentoft, F.C. (Eds.), Elsevier: Amsterdam, Netherlands, **2012**, pp. 127-239.
3. Perego, C.; Millini, R. Porous materials in catalysis: Challenges for mesoporous materials. *Chem. Soc. Rev.* **2013**, 42, 3956-3976.
4. Kadib, A.E.; Katir, N.; Finiels, A.; Castel, A.; Marcotte, N.; Molvinger, K.; Biolley, C.; Gaveau, P.; Bousmina, M.; Brunel, D. Mesostructured fatty acid-tethered silicas: Sustaining the order by co-templating with bulky precursors. *Dalton Trans.* **2013**, 42, 1591-1602.
5. Zhu, P.; Zhou, L.; Song, Y.; Cai, L.; Ji, M.; Wang, J.; Ruan, G.; Chen, J. Encapsulating insoluble antifungal drugs into oleic acid-modified silica mesocomposites with enhanced fungicidal activity. *J. Mater. Chem. B* **2020**, 8, 4899-4907.
6. Doadrio, J.C.; Sousa, E.M.; Izquierdo-Barba, I.; Doadrio, A.L.; Perez-Pariente, J.; Vallet-Regí, M. Functionalization of mesoporous materials with long alkyl chains as a strategy for controlling drug delivery pattern. *J. Mater. Chem.* **2006**, 16, 462-466.
7. Quang, D.V.; Lee, J.E.; Kim, J.K.; Kim, Y.N.; Shao, G.N.; Kim, H.T. A gentle method to graft thiol-functional groups onto silica gel for adsorption of silver ions and immobilization of silver nanoparticles. *Powder Technol.* **2013**, 235, 221-227.

8. Hornebecq, V.; Antonietti, M.; Cardinal, T.; Treguer-Delapierre, M. Stable silver nanoparticles immobilized in mesoporous silica. *Chem. Mater.* **2003**, *15*, 1993-1999.
9. Bromberg, L.; Chen, L.; Chang, E.P.; Wang, S.; Hatton, T.A. Reactive silver and cobalt nanoparticles modified with fatty acid ligands functionalized by imidazole derivatives. *Chem. Mater.* **2010**, *22*, 5383-5391.
10. Grinberg, S.; Kolot, V.; Mills, D. New chemical derivatives based on *Vernonia galamensis* oil. *Indus. Crop. Prod.* **1994**, *3*, 113-119.
11. Awoke, Y.; Chebude, Y.; Márquez-Álvarez, C.; Díaz, I. Solvent free epoxidation of vernonia oil using Ti-SBA-15 with tailor made pore size and particle morphology. *Catal. Today* **2020**, *345*, 190-200
12. Grinberg, S.; Linder, C.; Kolot, V.; Waner, T.; Wiesman, Z.; Shaubi, E.; Heldiman, E. Novel cationic amphiphilic derivatives from vernonia oil: Synthesis and self-aggregation into bilayer vesicles, nanoparticles, and DNA complexants. *Langmuir* **2005**, *21*, 7638-7645
13. United States Patent McClory et al. US 7.803,409 B2 (45) Date of Patent: Sep. 28, **2010**.
14. Desalegn, T.; Villar-Garcia, I.J.; Licence, P.; Díaz, I.; Chebude Y. Enzymatic synthesis of epoxy fatty acid starch ester in ionic liquid–organic solvent mixture from vernonia oil. *Starch/Stärke* **2014**, *66*, 385-392.
15. Shah, D.U. Towards sustainable polymers and plastics: NMR spectroscopic analysis and characterisation of vernonia seed (*Vernonia galamensis*) oil and epoxidised soya bean seed (*Glycine max*) oil. *The SciTech* **2014**, *01*, 13-29.
16. Christie, W.W. *Preparation of Ester Derivatives of Fatty Acids for Chromatographic Analysis, Advances in Lipid Methodology - Two*, Christie, W.W. (Ed.), Oily Press: Dundee; **1993**; pp. 69-111.
17. Deutsche Einheitsmethoden zur Untersuchung von Fetten, Fettprodukten, Tensiden und verwandten Stoffen, **2021**.
18. Chen, M.; Ding, W.H.; Kong, Y.G.; Diao, W. Conversion of the surface property of oleic acid stabilized silver nanoparticles from hydrophobic to hydrophilic based on host–guest binding interaction. *Langmuir* **2008**, *24*, 3471-3478.
19. Mavani, K.; Shah, M. Synthesis of silver nanoparticles by using sodium borohydride as a reducing agent. *Int. J. Eng. Res. Technol.* **2013**, *2*, DOI: 10.17577/IJERTV2IS3605.
20. Bromberg, L.; Chen, L.; Chang, E.P.; Wang, S.; Hatton, T.A. Reactive silver and cobalt nanoparticles modified with fatty acid ligands functionalized by imidazole derivatives. *Chem. Mater.* **2010**, *22*, 5383-5391.
21. Díaz, I.; Pérez-Pariente, J.; Sastre, E. Pore-size control of Al-MCM-41 materials by spontaneous swelling. *Stud. Surf. Sci. Catal.* **1999**, *125*, 53-60.
22. Gascón, V.; Díaz, I.; Márquez-Álvarez, C.; Blanco R.M. Mesoporous silicas with tunable morphology for the immobilization of laccase. *Molecules* **2014**, *19*, 7057-7071.
23. Serra, E.; Díez E.; Díaz, I.; Blanco, R.M. A comparative study of periodic mesoporous organosilica and different hydrophobic mesoporous silicas for lipase immobilization. *Micropor. Mesopor. Mater.* **2010**, *132*, 487-493.
24. Naik, S.P.; Bui, V.; Ryu, T.; Miller, J.D.; Zmierzak, W. Al-MCM-41 as methanol dehydration catalyst. *Appl. Catal. A* **2010**, *381*, 183-190.
25. Díaz, I.; García, B.; Alonso, B.; Casado, C.M.; Morán, M.; Losada, J.; Pérez-Pariente, J. Ferrocenyl dendrimers incorporated into mesoporous silica: New hybrid redox-active materials. *Chem. Mater.* **2003**, *15*, 1073-1079.